Contents lists available at ScienceDirect

Mechanical Systems and Signal Processing

journal homepage: www.elsevier.com

Obtaining manufactured geometries of deep-drawn components through a model updating procedure using geometric shape parameters

Vamsi Krishna Balla[a, b, *], Laurens Coox[a, c], Elke Deckers[a, c], Bert Plyumers[a, c], Wim Desmet[a, c], Kannan Marudachalam[b]

[a] *Machine Design and Automation (PMA), Department of Mechanical Engineering, Celestijnenlaan 300 – box 2420, 3001 Leuven, Belgium*
[b] *Research & Development, TVS Motor Company, Hosur, Tamil Nadu, India*
[c] *Member of Flanders Make, Belgium*

ARTICLE INFO

Keywords:
Modal updating
Modal Assurance Criterion
Optimization
Deep drawing

ABSTRACT

The vibration response of a component or system can be predicted using the finite element method after ensuring numerical models represent realistic behaviour of the actual system under study. One of the methods to build high-fidelity finite element models is through a model updating procedure. In this work, a novel model updating method of deep-drawn components is demonstrated. Since the component is manufactured with a high draw ratio, significant deviations in both profile and thickness distributions occurred in the manufacturing process. A conventional model updating, involving Young's modulus, density and damping ratios, does not lead to a satisfactory match between simulated and experimental results. Hence a new model updating process is proposed, where geometry shape variables are incorporated, by carrying out morphing of the finite element model. This morphing process imitates the changes that occurred during the deep drawing process. An optimization procedure that uses the Global Response Surface Method (GRSM) algorithm to maximize diagonal terms of the Modal Assurance Criterion (MAC) matrix is presented. This optimization results in a more accurate finite element model. The advantage of the proposed methodology is that the CAD surface of the updated finite element model can be readily obtained after optimization. This CAD model can be used for carrying out analysis, as it represents the manufactured part more accurately. Hence, simulations performed using this updated model with an accurate geometry, will therefore yield more reliable results.

1. Introduction

Numerical computational tools like the Finite Element Method (FEM) proposed by Zienkiewicz [1] have become very powerful in aiding the design of structural systems. As some very important decisions – cost, weight and design finalization – will be made based on the results of the simulations using the finite element (FE) models, it is extremely important to develop FE models that are accurate representations of their physical counterparts. Therefore, correlation and validation of the behavior of real structural systems with corresponding numerical models is very important. The crucial importance of physical experiments through which one can understand the behavior of actual systems cannot be overstated. Numerical simulations can only complement physical experimentation

* Corresponding author at: Machine Design and Automation (PMA), Department of Mechanical Engineering, Celestijnenlaan 300 – box 2420, 3001 Leuven, Belgium.
Email address: vamsikrishna.balla@kuleuven.be (V.K. Balla)

http://dx.doi.org/10.1016/j.ymssp.2017.05.009
Received 17 January 2017; Received in revised form 10 April 2017; Accepted 7 May 2017
Available online xxx
0888-3270/

but cannot totally replace them. Once a modeling methodology has been proven to mimic experimental observation, numerical simulations using the proven methodology could be a powerful route to design of actual systems.

Building reliable FE models of mechanical and structural systems to carry out dynamic analysis can be quite complex. The sources of errors in modeling these systems may have frequency dependence. The impact of these errors – inaccurate loads, boundary conditions, and system characteristics – on the system behavior gets amplified with increasing frequency. Further, though one could obtain reasonably good quality numerical models of individual components, getting a good quality system-level models is more difficult due to poor interface (connector) modeling.

Traditionally, modal updating using material properties – Young's modulus, material density and damping ratio – was used by various researchers in order to validate FE models. Mottershead et al. [2], published a literature review on modal parameter updating. Mottershead et al. [3] proposed an eigenvalue sensitivity approach to update FE models to model welded joints accurately. Yuan et al. [4] proposed a more accurate two stage modal updating. The stiffness and mass matrices are updated first, followed by updating with damping. More recently, Ning Guo et al. [5] demonstrated that the strain-based FRF updating procedure is more accurate compared to a modal parameter updating procedure. Maletta et al. [6] proposed a method, using a finite element model and Genetic Algorithms (GA), to obtain elastic constants of composite laminates. Meruane [7] proposed a methodology to identify anti-resonances using transmissibility functions. The anti-resonances of finite element model were updated using a GA based optimization method. Petrone et al. [8] carried out model updating of a composite panel made of unidirectional flax fibres embedded in a polyethylene matrix (flax-PE) flat panel. They updated the mechanical properties, used in the FE model, using an inverse modelling method based on parallel genetic algorithms in order to obtain the minimum difference between the numerical and experimental data. It can be seen that the modal parameter based approaches are well suited for updating of assembly-level FE models, so as to model interface properties of joints, bushings and welds properly.

In case of components (with high draw ratios) manufactured through a deep drawing process, where typically no joint exists, modal updating using material properties alone won't be sufficient to achieve the desired accuracy in predictions. Andersson et al. [9] carried out both numerical and experimental work to evaluate spring back of an automobile front side member. They studied the effect of different materials on spring back. They found up to 7.5 mm profile deviation from the original CAD profile happened due to spring back effect. Hancock et al. [10] showed that part-to-part variation contributed with 21% of total variation. This variation was primarily because of random spring back associated with the process. Kim et al. [11] showed that spring back of 4 mm was very likely for an automobile motor-case with 40 mm radius. Hence they resorted to process improvement by implementing multi-forming along with elliptical core for reduction of spring back. They were able to achieve an excellent reduction in spring back value of 0.038 mm with redesigned elliptical core. de Souza et al. [12] carried out stochastic simulations to quantify the contribution of process parameters – Blank Holder Pressure (BHP) and coefficient of friction – and mechanical material properties – Yield stress and Ultimate strength – on spring back of an auto-mobile component. They showed changes in process parameters resulted in changes in strain component thus effecting the magnitude of external work applied to forming system. Material property variation, on the other hand, effected stress component of the response. Padmanabhan et al. [13] studied thickness variation of a LPG bottle manufactured through deep drawing process. The main objective of their study was to reduce thickness variation in the deep drawn part, i.e. to maximize the minimum thickness. They proposed various blank holder force strategies – highest, lowest, optimal, linearly increasing, linearly decreasing and adaptable. Their study indicated that about 25% thickness reduction happened when the highest blank holder force was applied. The required component thickness was achieved when optimum BHP was used. Mouatassim et al.[14] used PAM STAMP software to analyze thickness variation of a dash-pot cup of the RENAULT Twingo. It was found from their study that about 10% thickening and 20% thickening happened at the critical locations.

It can be seen from the work done by above researchers that significant geometry profile and thickness variations occur in the components manufactured by deep drawing. Hence, modal updating of FE models using material properties alone will not be sufficient to achieve the desired accuracy in predictions. According to the best of authors' knowledge, there is no literature that addresses updating procedures taking profile and thickness variations into account which occur in deep drawing process. In this research work, a novel method of modal updating is proposed by incorporating geometry shape variables, defined using morphing of the finite element model obtained from the original CAD, which mimic changes happened during the manufacturing process, to construct the deviated profile of component. Modal Assurance Criterion (MAC) based optimization is carried out using combination of a FE solver and an optimization solver that uses the GRSM algorithm. Matlab [15] is used as a simulation manager in order to run the FE morphing software and optimization solvers. The advantage of the proposed methodology is that the CAD surface of the updated modal model can be obtained. This CAD model can be used to design die and punch for successive designs or for carrying out numerical analysis, as results of such updated part analysis will be more accurate than those of analysis results where the finite element model is obtained from the original CAD model. The outline of the paper is as follows – In the first and second sections of paper, a brief theoretical description of modal updating and geometry based shape parameter updating procedure is given. An industrial application oriented component – an oil-pan look-a-like – is designed and manufactured using a deep-drawing manufacturing process. It is demonstrated by incorporation of geometry shape variables, a reliable finite element model can be obtained through optimization. Finally, the procedure to obtain an updated CAD model of the manufactured component using geometry based shape parameter optimization is discussed in the subsequent sections. The authors also envisage IsoGeometric Analysis (IGA) on this case of problems to arrive at an accurate description of the actual geometry as a future research work.

2. Review of modal updating

2.1. Conventional methods

In this section, a brief review on theory of modal updating is discussed. The modal updating concept was introduced by Ewins [16], Heylen et al. [17] and O' Callahan [18]. The correlation between FE and experimental modes can be established by the Modal Assurance Criterion (MAC). The MAC value for a pair of modal vectors $\{\phi_r\}_i$ and $\{\phi_a\}_j$ is a scalar number, that indicates the degree of consistency between these two vectors, and was defined by Allemang and Brown [19] as follows:

$$MAC = \frac{|\{\phi_r\}_i^H \{\phi_a\}_j|^2}{(\{\phi_r\}_i^H \{\phi_r\}_i)(\{\phi_a\}_j^H \{\phi_a\}_j)}, \tag{1}$$

where $\{\}^H$ denotes the Hermitian matrix. A value close to unity indicates a good correlation between the experimental mode shape $\{\phi_r\}_i$ and the FE computed eigenvector $\{\phi_a\}_j$. Modal updating is broadly classified into two categories:

- In direct FE model updating methods, Lagrange multipliers are derived from an optimisation study while minimising an objective function along with additional constraints such as the system symmetry and the orthogonality conditions. Baruch [20] corrected the system stiffness matrix whereas Berman and Nagy [21] proposed an equation to identify the differences in the system mass matrix. This method is not widely used, as it demands large volume of accurate experimental data.
- In iterative FE model updating methods, design parameters are updated on an elemental basis of a parametrized FE model for reducing the error using the following equation

$$[S]\{\varphi\} = \{\epsilon\}, \tag{2}$$

where [S] is the sensitivity matrix as suggested by Fox et al. [22], $\{\varphi\}$ the changes in updating parameters and $\{\epsilon\}$ the error, the difference between the measured and predicted dynamic properties. The eigenvector sensitivities cannot be solved in closed form and must therefore be approximated as suggested by Henning [23]. The eigenvector sensitivities are generally orders of magnitude smaller than the eigenvalue sensitivities, which leads to ill-defined sensitivity matrices [S]. Chen and Garba [24] proposed an over-determination method to solve this problem.

2.2. Geometry shape parameter based updating

The finite element mesh-based morphing model is suitable for carrying out optimization. It is found from literature that surface deformation models are most commonly used for carrying out design optimization of sheet metal surfaces such as car bodies, aircraft wings and ship hulls. In this morphing method – the domain handle approach as suggested by Daniel et al. [25] (brief overview of theory is mentioned and the reader is referred to their paper for detailed explanation) – three types of surface regions are defined on the mesh: (i) the handle region H that is displaceable (ii) fixed region F which is constrained (iii) the deformable region D is updated according to the physical deformation method while satisfying the Dirichlet constraints given by H and F. The deformable region D should behave in a physically-plausible manner, i.e., it should deform like a thin shell based on stretching and bending energies. The deformations occurring in design optimization tasks typically are rather small. Therefore, a linear deformation model will be sufficient, where stretching and bending are measured by first and second order partial derivatives of the displacement function d, respectively. In the continuous setting, the deformation $d : S \rightarrow R3$ of a surface S can be computed by minimizing the energy functional

$$E_{shell}[d] = w_s E_{stretch}[d] + w_b E_{bend}[d] + w_f E_{flx}[d], \tag{3}$$

consisting of weighted energy contributions for stretching, bending and constraint deviation

$$E_{stretch}[d] = \int_D \|\nabla d(x)\|^2 \, dx, \tag{4}$$

$$E_{bend}[d] = \int_D \|\Delta d(x)\|^2 \, dx, \tag{5}$$

$$E_{flx}[d] = \int_{H \cup F} \left\|d(x) - \bar{d}(x)\right\|^2 dx, \tag{6}$$

where ∇d denotes the Jacobian of d, $\Delta d = \nabla \cdot \nabla d$ its Laplacian, $\|.\|$ the Frobenius matrix norm or the Euclidean vector norm and $\bar{d}$ the prescribed Dirichlet constraints for the fixed and displaceable handle regions. The surface S is discretized by a proper triangular mesh M and hence the most flexible discretization of thin shell deformation is one whose degrees of freedom are the individual ver-

tex positions $x_1, x_2 \ldots .. x_n$ or the vertex displacements $d_1, d_2 \ldots .. d_n$

$$d_h(x) = \sum_{i=1}^{n} d_i \psi_i(x), \tag{7}$$

where ψ_i are the piecewise linear shape functions on the triangulation M. Based on the discretization we can approximate the above energies as

$$E_{stretch}[d_h] = \sum_{x_i \in D} A_i \left\| \nabla d_i \right\|^2, \tag{8}$$

$$E_{bend}[d_h] = \sum_{x_i \in D} A_i \left\| \Delta d_i \right\|^2, \tag{9}$$

$$E_{flx}[d_h] = \sum_{x_i \in H \cup F} A_i \left\| d_i - \bar{d}_i \right\|^2, \tag{10}$$

where A_i denotes the Voronoi area of vertex i, and where we use the well-established discrete differential operators proposed by Meyer et al. [26]. These allow to write the discrete gradient ∇d_i and discrete Laplacian Δd_i as a linear combination of neighbouring vertices. For implementation convenience and easier extensibility in the following sections, the discrete shell energy is expressed as

$$E_{shell}[d_h] = w_s \left\| Gd \right\|^2 + w_b \left\| Ld \right\|^2 + w_f \left\| F(d - \bar{d}) \right\|^2, \tag{11}$$

where $d = (d_1^T \ldots, d_n^T)^T$ is the $(n \times 3)$ matrix or per-vertex displacements and G and L are gradient and Laplace matrices containing the required cotangent weights in each row and having their row weighted by $\sqrt{A_i}$ respectively. F is a diagonal matrix with $F_{i,i} = \sqrt{A_i}$ if $x_i \in F \cup H$ and $F_{i,i} = 0$ otherwise. The minimization of shell energy requires, to solve the normal equation of the linear least squares system

$$(w_s G^T G + w_b L^T L + w_f F^T F) d = w_f F^T F \bar{d}, \tag{12}$$

The shape deformation will be controlled by an interface that specifies displacements for certain surface regions. In this the user can directly manipulate certain regions of the surface mesh. However, direct manipulation interfaces are preferable for design optimization, since the direct coupling between optimization parameters and the effect on the design variation leads to improved convergence rates.

In the present work, some individual and combinations of likely geometry deviations from the nominal part dimensions are created using morphing of the finite element model obtained from the original CAD, which are named as geometry shape parameters. The initial modal analysis is carried out using the above mentioned finite element model, in which geometry shape parameters are defined. These geometry shape parameters are used in subsequent optimization studies that employ the GRSM method. In the optimization study, these geometry shape variables are varied at three levels, whose limits are obtained from nominal and scanned models.

3. Results and discussions

3.1. Initial CAD design and finite element results

An industrial look-a-like application component with high draw ratio is designed as shown in Fig. 1. This component is designed with several flat surfaces in order to have localized mode shapes. The component modelling and meshing is carried out in a CAD software and in a standard FE pre-processing software, respectively. The component has a thickness of 1.5 mm and is made up of IS 513 CR0 grade. The density, modulus of elasticity and Poission ratio of the material are 7850 kg/m^3, 2.1 $\times 10^5$ MPa and 0.3, respectively. The mass of the component is 4.6 kg. The finite element model mesh consists mainly of bilinear quadrilateral shell elements with linear shape functions along with few triangular elements in order to reduce the discretization error. The component mesh has 12092 nodes and 12422 elements. An element size of 6 mm is used in order to achieve mesh convergence. The accelerometer mounted during experiments, has a mass of 10.5 g. This weight is accounted for in the FE model by adding CONM2 mass elements at the corresponding nodes. The modal analysis of the component in free-free and clamped boundary conditions is carried out using OptiStruct [27] software. In practice, for the clamped boundary conditions, the component is fixed at ten holes that are located symmetrically to the YZ plane (shown in Fig. 1) with M10 bolts. A pressure film is placed between the component and the fixing surface in order to obtain the contact pressure pattern. This contact pressure pattern reveals that the area around the holes has zero displacement. Hence, in the FE model the Degrees Of Freedom (DOF) of the nodes around the circular holes are completely constrained to model the clamping conditions and to have a good representation of the real setup. The component natural frequencies in free-free and clamped condition are shown in Table 1. The component mode shapes in clamped boundary condition are shown in Fig. 2. It can be seen from the mode shapes that deformation is very local at almost all of the natural frequencies except at the fundamental

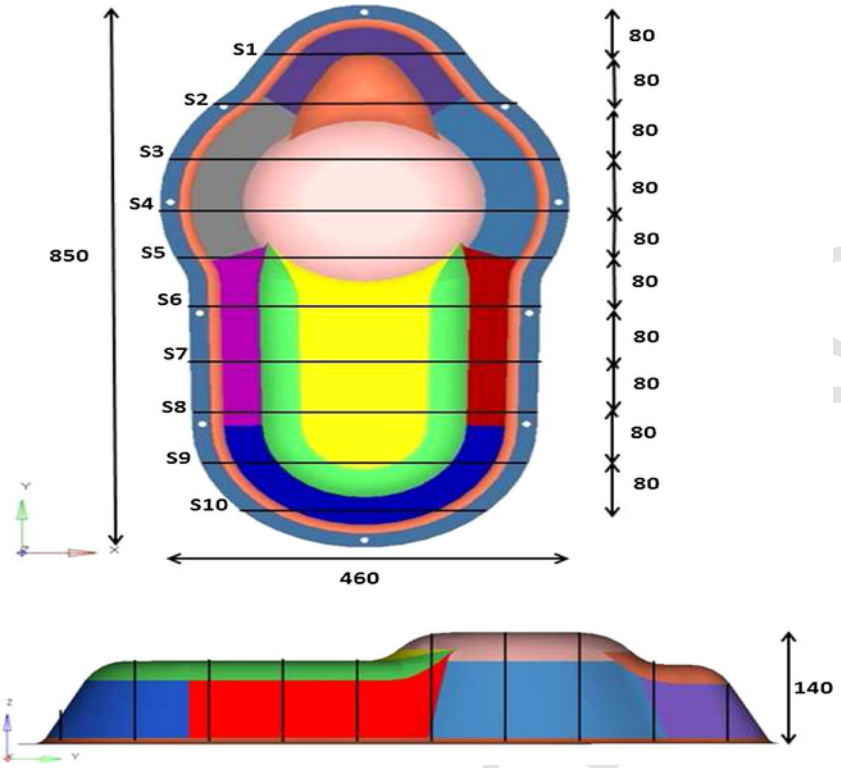

Fig. 1. The front and top views of nominal component (dimensions are in millimeters.)

Table 1
Comparison of natural frequencies (Hz) in free-free and clamped boundary conditions.

Mode No.	Free-Free			Clamped		
	FE	Experiment	% difference	FE	Experiment	% difference
1	90	91	1.1	248	254	4.6
2	110	114	3.5	255	298	14.4
3	242	247	2.0	398	409	2.7
4	252	271	7.0	426	432	1.4
5	303	327	7.3	438	448	2.2
6	373	353	−5.7	460	461	0.2

frequency, where the mode shape is global in nature. A node-set of 102 points, representing the complete geometry, is identified for defining test geometry and for also computing the MAC between finite element and experimental results.

3.2. Manufacturing process

The component is manufactured in a single-step deep drawing process. The punch, blank holder plate and die are shown in Fig. 3. As the component is large, it posed some problems while manufacturing through conventional deep drawing arrangement where a punch travels vertically down to press blank material into a die. This challenge is overcome by fixing the heavy punch to the ground while the blank material – firmly held between blank holder plate and die – is pressed on the same to form the component using a die. The punch, die and blank holder plate are made up of mild steel i.e. medium carbon steel (EN8), as it is easily machinable. A hydraulic press, model HD 3146 from BEMCO Hydraulics with 315 ton capacity, is used for manufacturing this component. The process parameters played a significant role in obtaining a component that is free from wrinkles and cracks. As can be seen from the Fig. 1, the component has a wall angle of 55° which potentially can cause spring back due to elastic recovery upon unloading of the tool. Also as the component geometry is complex and has higher depth, manufacturing resulted in substantial thickness and profile variation. This fact is ascertained by measuring the manufactured geometry through optical scanning that used photogrammetric techniques to acquire point cloud data of the part. Optical scanning is performed using a GOM ATOS I scanner [28]. The component surface is prepared with white spray to avoid any possible reflections while scanning. Also several small marker stickers, that allow to merge optical scans of different regions, are attached to the component along with some larger stickers that are used as a global reference. The scanning is done on both sides of component, which allowed to perform thickness variation analysis. The component

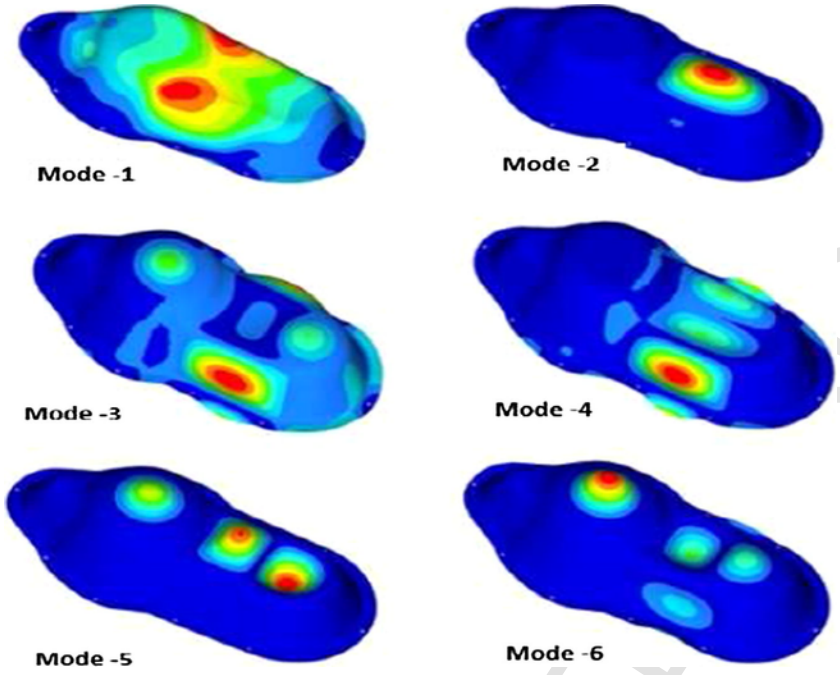

Fig. 2. Component modeshapes in constrained boundary condition.

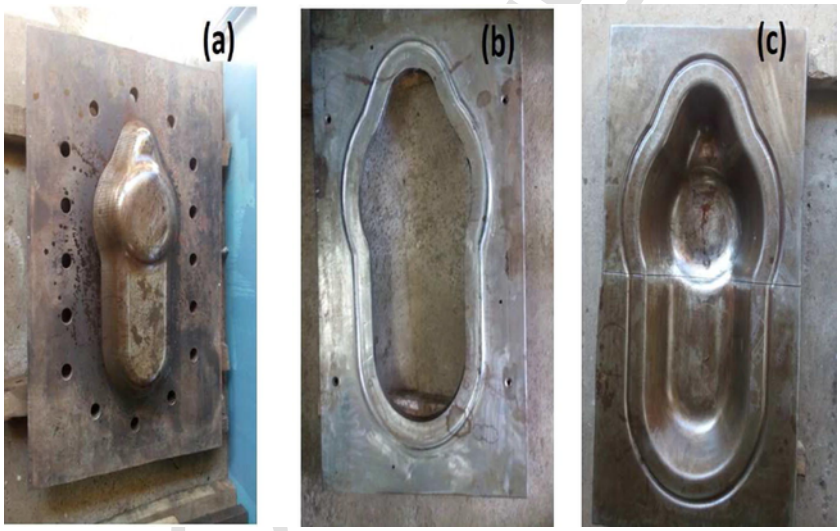

Fig. 3. Typical set-up of component manufacturing (a) Punch, (b) Blank Holder Plate, (c) Die.

surface is modelled using the cloud point data obtained through scanning. It is observed, as shown in Fig. 4, that significant profile deviation and thickness deviation from the original CAD component has taken place.

3.3. Experimental results

The component modal testing is carried out in both free-free and clamped boundary conditions. In case of free-free modal testing, the component is suspended using four bungee cords as shown in Fig. 5 and it is clamped at ten holes using M10 bolts onto ground to simulate a clamped boundary condition. The modal testing included 102 impact locations (same set of points that are identified in the finite element model described in the Section 3.1) of the test object to be able to avoid any spatial aliasing of modes in the frequency range of interest. An impact testing using a roving hammer (Onosokki GK 3100) technique is chosen for carrying out modal testing in order to avoid mass-loading effects on this thin sheet metal component. The component is impacted at 102 points in the normal direction to each surface. The accelerations at response locations are measured using five tri-axial (PCB 356A02 type) accelerometers. These accelerometers have a frequency range valid up to 5000 Hz with ±5% error and lowest transverse sensitivity. A

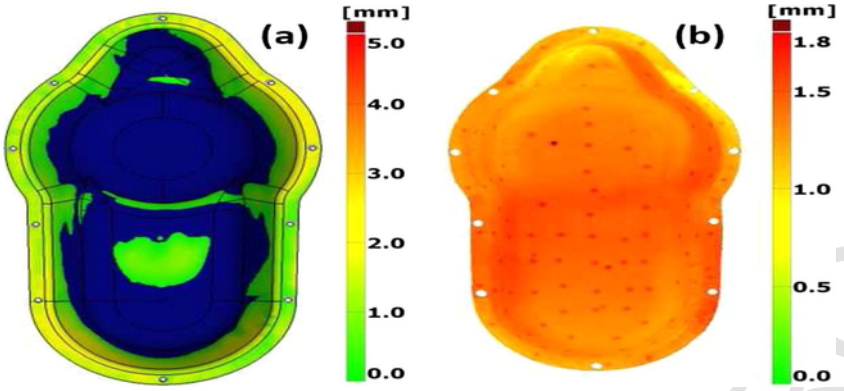

Fig. 4. Actual component (a) profile deviation, (b) thickness distribution.

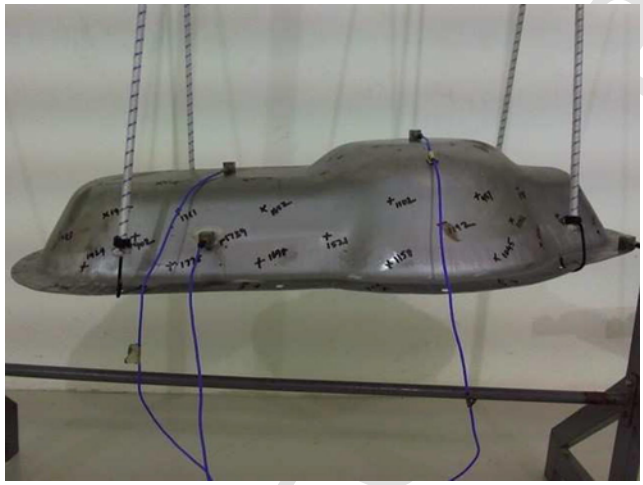

Fig. 5. Test set-up of modal testing of component in free-free boundary condition.

total weight of 52.5 g is added to the structure during modal testing as each accelerometer weighs 10.5 g. A force window (1%) on the impact input signal and a Hanning window for response is used to minimize noise in the response signal. Besides, it was decided to have ten averages at each impact location to obtain and averaged FRF in order to minimize noise. These averaged FRFs at each node is used in curve-fitting of the modal data to obtain eigenfrequencies and mode shapes. The five response locations are selected such that they are not nodal points (where displacement amplitude is minimum) – from the finite element results – throughout the frequency range of interest. Also, in case of clamped boundary condition modal testing, the same reference and response locations are used. The sampling frequency used for acquiring data is 4098 Hz along with 0.5 Hz frequency resolution. The hardware used for data acquisition is LMS SCADAS SCM-05 [29] and LMS Test.Lab [30] software is used for carrying out modal test data analysis. The eigenfrequency and modeshapes of the component for both sets of boundary conditions are obtained after carrying out curve-fitting of modal test data. It is decided to carry out modal updating for the modes in the frequency range of 0–1000 Hz. Hence, the first 15 eigenfrequency and modeshapes for free-free testing results and 12 eigenfrequency and modeshapes for clamped condition are obtained. It is possible to arrive at a single sum frequency response function (FRF), (by squaring the magnitudes at each frequency and then summing up for all FRFs) to represent the component behaviour. This frequency response function characterizes the dynamic behaviour of the component in an average sense. It may be noted that this metric is useful only for frequency-representation of component.

3.4. Comparison of initial results

The frequency and mode shape results obtained in previous sections through finite element simulation and modal testing are compared. In order to assess the validity of finite element results, the sum of FRFs of 102 points is compared with that of experimental results. It can be seen from Fig. 6, that there is a reasonable match between experimental and simulation frequency response functions for both boundary conditions. As mentioned in previous sections, the MAC is computed at 102 locations of the component to understand modeshape match. The MAC between simulation and experimental results for the free-free configuration, as shown in Fig. 7(a) is poor, especially after the first five mode shapes. It can be seen that MAC for the clamped boundary condition configura-

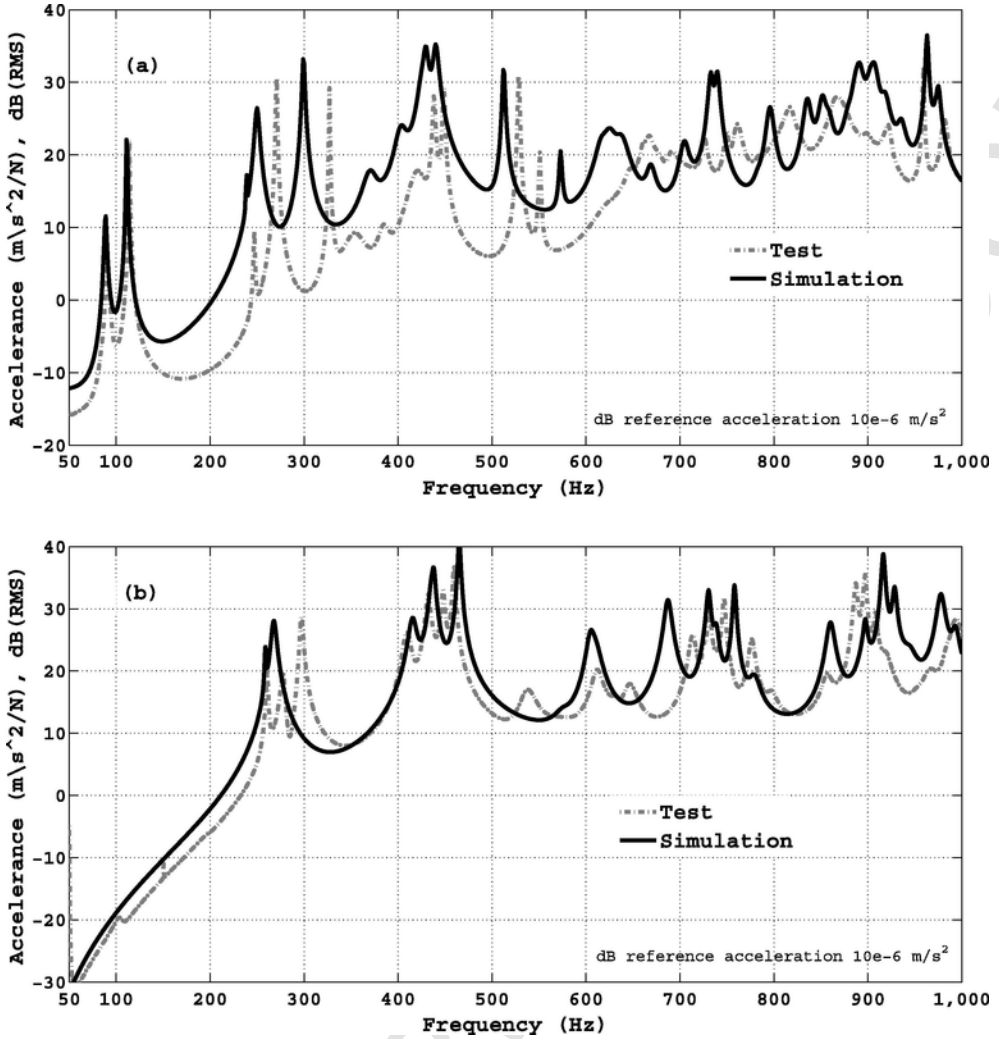

Fig. 6. Comparison of sum of Frequency Response Functions (FRFs) at 102 locations between simulation and experimental results in (a) free-free, (b) clamped boundary conditions.

tion is even worse as shown in Fig. 7(b). It can be seen from the above results that a precise geometry and local dynamics information are needed to be able to get good frequency and MAC correlation.

3.5. Sensitivity analysis & optimization procedure

In the following section, the procedure to define the geometry shape variables is explained. A sensitivity analysis of the material properties and shape variables is carried out to identify the most sensitive groups. The optimization study, that included the geometry shape variable, is shown to result in a reliable finite element model.

3.5.1. Geometry shape parameter definition and sensitivity analysis

In the current research work, the methodology followed to obtain a reliable dynamic equivalent finite element model and the corresponding CAD model that represents the actual physical prototype is described using a flowchart as shown in Fig. 8. As shown in the flowchart, a finite element model is obtained using the original CAD model and the same is analyzed for finding eigenfrequencies and modeshapes. These FE frequencies and modeshapes are correlated with respective experimental results using two metrics – sum of FRFs and MAC matrix – in order to access the FE model accuracy. The finite element model morphing technique is used in order to model profile variation using geometry shape variables. The theory of creation of these geometry shape variables is explained in earlier Section 2.2. These geometry shape variables are small nodal perturbations that can mimic the profile changes that happen during the manufacturing of the component due to the change in process parameters and random phenomenon like spring back. Typical shape variable deformations are shown in Fig. 9. It may be noted that during the actual optimization study, the magnitudes of these perturbations are very small and their limits are obtained from the actual scanned geometry. The selection of six cru-

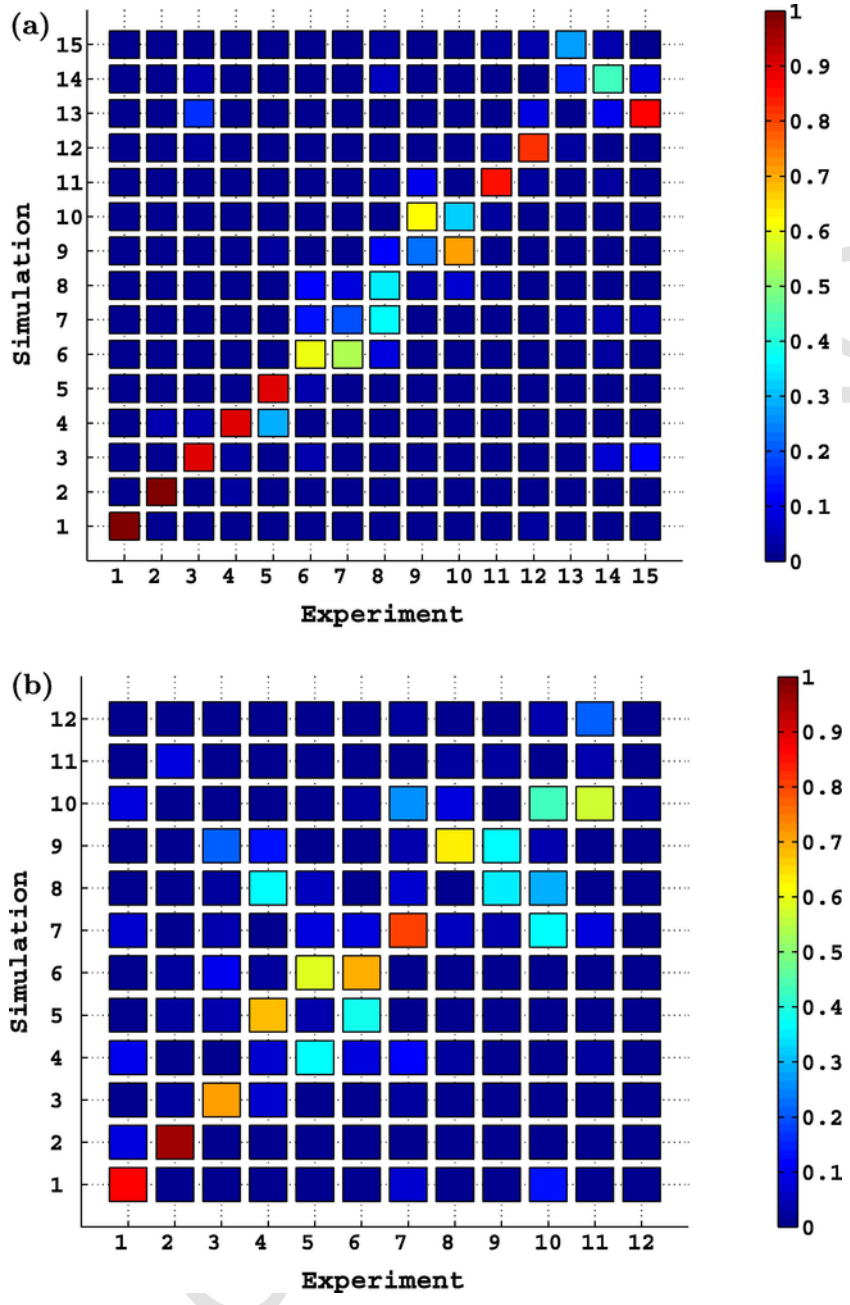

Fig. 7. Baseline MAC results (a) free-free, (b) clamped boundary conditions.

cial geometry shape variables for the optimization study is preceded by a design sensitivity analysis and Design Of Experiments (DOE). In the initial analysis phase, twelve geometry shape variables (corresponding to each surface of the component, shown in twelve different colours in Fig. 1) are defined. It is assumed that by using individual or a combination of these geometry shape variables allows to arrive at the deviated geometry starting from the nominal CAD surfaces of the component. This fact will be ascertained in the subsequent sections where deviated geometry is re-constructed using critical geometry shape variables identified in the sensitivity analysis. In the initial phase, geometry shape variables are defined using heuristic engineering knowledge of the manufacturing process. Hence a sensitivity analysis is carried out to understand the most significant geometry variables.

The variation of the first and second diagonal terms of MAC matrix with respect to lower, initial and upper bounds of a geometry shape variable is shown in Figs. 10 and 11 respectively. It may be noted that the slope of MAC variation line is defined as sensitivity of a particular shape variable. It can be seen from the above results that only few geometry shape variables are having a higher sensitivity. However, results are shown only for the first two diagonal terms of the MAC matrix to avoid repetitious nature of results. In order to understand these shape variable sensitivities for other MAC values i.e. up to the first twelve diagonal terms of MAC matrix,

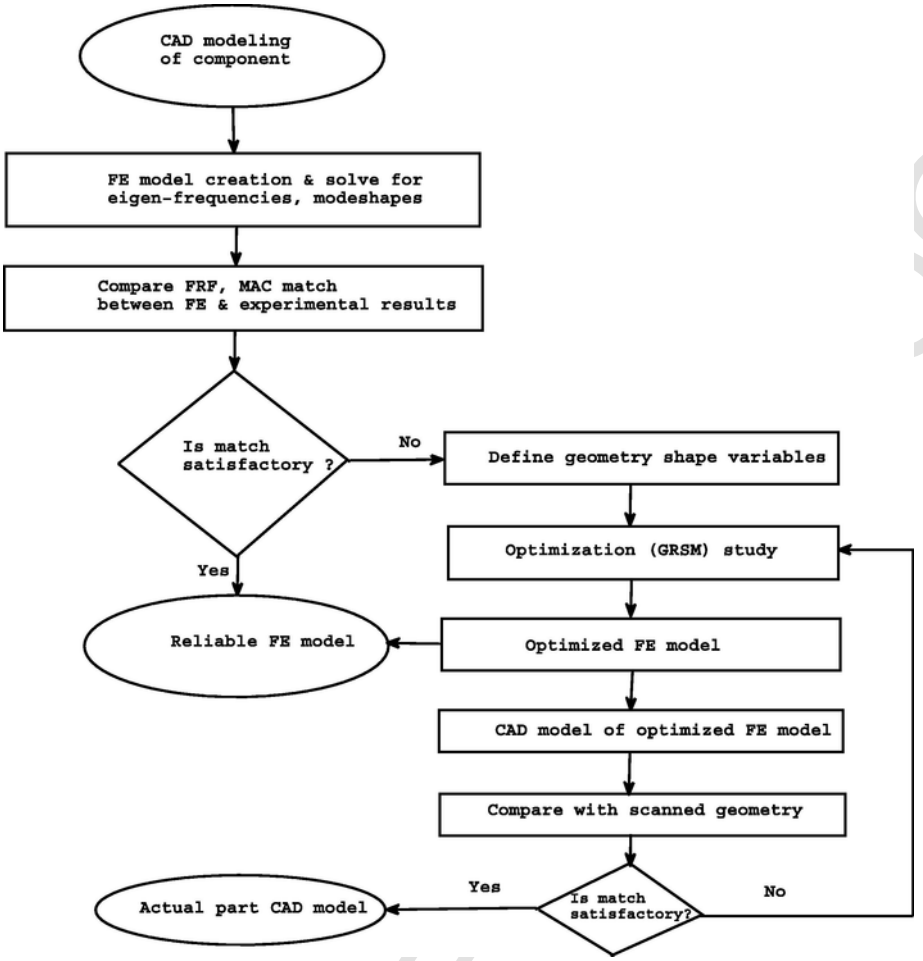

Fig. 8. Flowchart describing the process to obtain the actual part geometry and a reliable FE model.

a sensitivity matrix is computed for both free-free and clamped boundary conditions. These results are shown in Fig. 12. In this figure, geometry shape variables are plotted on x-axis and an absolute values of sensitivities on y-axis. In order to identify the most significant geometry shape variables, a histogram shown in Fig. 13 is computed for the first twelve diagonal terms. It can be seen from the figure that only six shape variables are significant. Hence these identified six geometry shape variables are considered in optimization studies.

A full factorial Design of Experiments (DOE) study is carried out by varying these crucial geometry shape variables at three levels. These six geometry shape variables are varied at three levels – lower bound, initial and upper bound – during the optimization study. In this optimization study, the initial bound represents the nominal surface that is same as the nominal CAD surface. The lower and upper bounds of geometry shape variable represent the deviation of surface on negative and positive side of nominal surface normal. A snake view result summary of DOE results are shown in Fig. 14. It may be noted from the results that shape variables are to be kept at lower and upper bounds to maximize diagonal terms of MAC matrix. It is seen from the results that shape variables 2,3,4 & 6 are to be kept at upper bound where as shape variables 1 & 5 are to be kept at lower bound to obtain highest MAC values for most modeshapes.

3.5.2. Optimization results

An optimization problem is formulated to maximize the diagonal terms of a MAC matrix. It is also essential to ensure that only one FE modeshape would correlate well with one of the experimental modeshapes. This can be achieved by minimizing the off-diagonal terms of the MAC matrix. This one-to-one modeshape match is expected, as care is taken during selection of node-set for computing MAC between FE and experimental results, to avoid spatial aliasing. Hence, the current optimization scheme objective is to maximize the diagonal terms of MAC matrix and also to minimize the off-diagonal terms. The following equations define the objective and constraint functions used in the optimization:

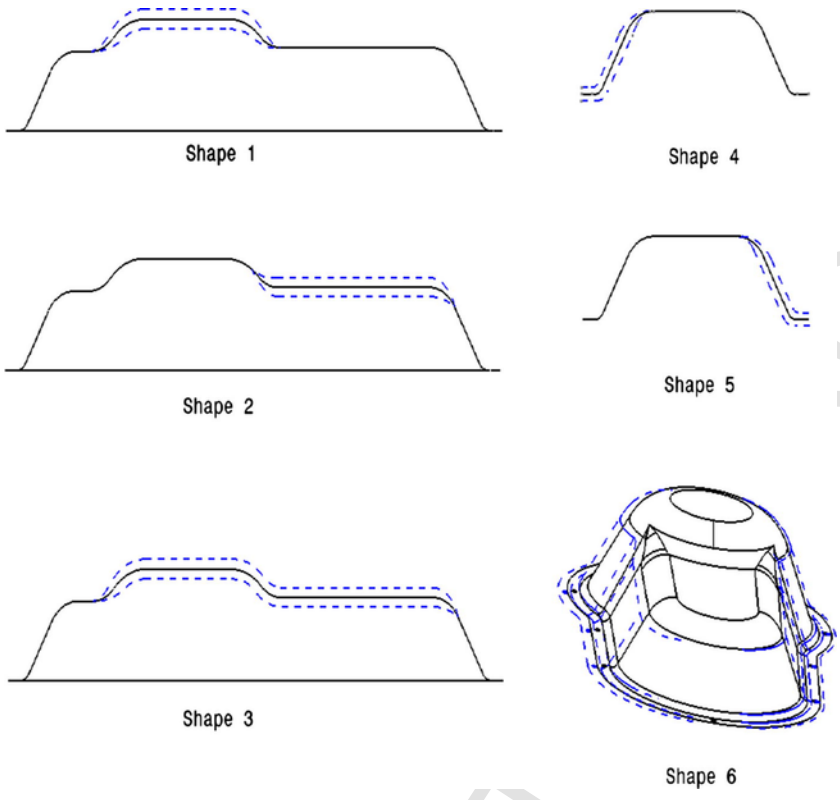

Fig. 9. Typical shape variables – dotted lines represent lower and upper bounds of deviated profile – used in optimization study.

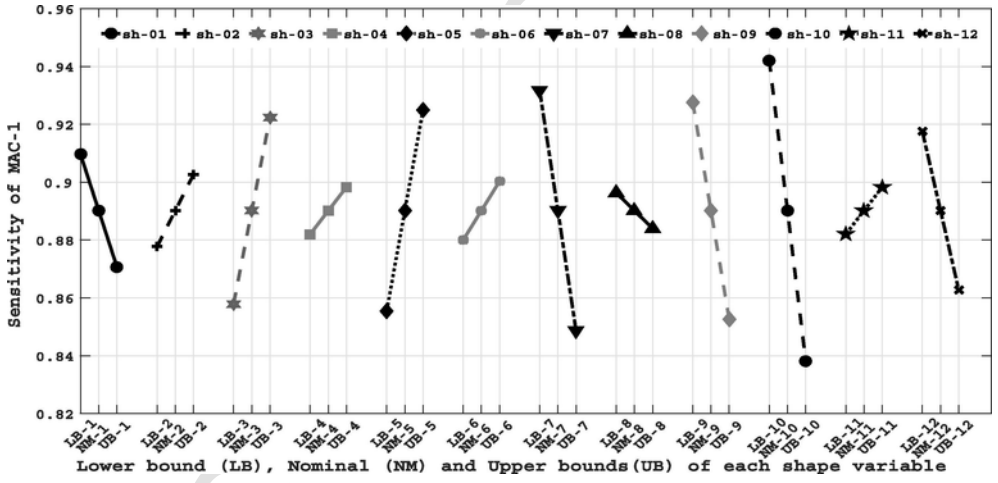

Fig. 10. Sensitivity results of different geometric shape variables of MAC-1 in the clamped boundary condition.

$$\max\ L_{obj} = \sum_{i=1}^{12}\sum_{j=1}^{12}\delta_{ij}\,M(i,j) \tag{13}$$

and

$$\min\ \gamma = \sum_{i=1}^{12}\sum_{j=1}^{12}M(i,j) - \sum_{i=1}^{12}\sum_{j=1}^{12}\delta_{ij}\,M(i,j) \tag{14}$$

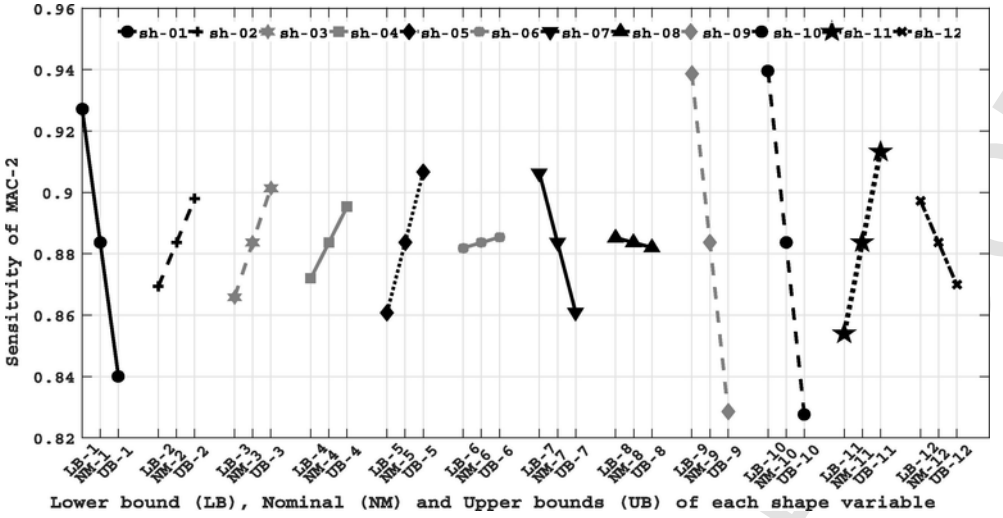

Fig. 11. Sensitivity results of different geometric shape variables of MAC-2 in the clamped boundary condition.

where M is MAC matrix, δ_{ij} is kronecker delta and is defined as follows:

$$\delta_{ij} = \begin{cases} 1, & \text{if } i = j, \\ 0, & \text{if } i \neq j. \end{cases}$$

In this work, GRSM is chosen as an optimization method. This method employs a robust search algorithm which is good at capturing global trends by avoiding the local maxima traps. The gradient based optimization methods although are efficient, these techniques suffer from disadvantage of strong dependence on an initial design. GRSM combines an adaptive Response Surface Method (RSM) optimization with global search. GRSM generates an initial response surface from the design space with a small number of designs. The optimum on this surface is compared with the exact solution. The algorithm will not converge in case of an error between the RSM and the exact solution. The algorithm generates some more new samples after updating the response surface. This is repeated until the user-defined number of designs are evaluated. It is seen that GRSM converges faster [27] in comparison to other optimization methods like Adaptive Response Method (ARSM) and GA. This optimization procedure is an iterative method to arrive at global approximations more accurately. This method uses higher order polynomials to approximate the optimization problem. Hence it is suitable for carrying out non-linear and multi-objective optimization.

The initial design space for optimization study is defined by geometry shape variables, Young's modulus, density and thickness. The component is divided into twelve segments,depicted with twelve different colors, as shown in Fig. 1. A representative Young's modulus, density, thickness of each segment along with twelve geometry shape variables that amounts to a total 48 variables (4×12 of ρ, t, E and geometry variables) are considered for the initial optimization study. The upper and lower bounds of Young's modulus and density are defined as ±10% of their nominal values for the optimization study. The upper and lower bounds of thickness variable and geometry shape variables are defined as ±20% of initial blank thickness and nominal surface position. The optimization study is performed in HyperStudy. A Matlab program is written to compute MAC values which interfaced with OptiStruct and HyperStudy to achieve the objective.

In the present study, the objective is to maximize MAC values for the first twelve modes i.e to achieve a MAC value of 0.8 or higher value, whichever is feasible. The optimization method, involved a mode-tracking option which ensured the MAC computation of corresponding mode shapes between initial and subsequent-run mode results. The optimization procedure involved options to continue with subsequent runs, in case of a failed run due to elemental quality errors or due to violations of constraints. The maximum number of runs are fixed to 5000, as this is found to be sufficient to achieve the convergence criterion during initial phase of optimization runs. The computational time is 72 h on a 16 GB Windows machine with 2.5 GHz processor and with 16 cores. A Matlab program is written to compute maximization of diagonal terms and minimization of non-diagonal terms from the optimization results that employed least-square method. The initial optimization results for free-free and clamped boundary conditions are shown in Figs. 15 and 16 respectively. As can be seen from the figures, the optimization study results in a good correlation between experimental and FE results. It may be noted that correlation is good for more modes in the case of free-free boundary condition as compared to clamped boundary condition.

In order to confirm the importance of geometrical shape variables, a second optimization – only material properties like Young's modulus, density and thicknesses – study is set-up with less variables in which geometric shape variables are excluded. As can be seen from Fig. 17, that correlation between simulation and experimental results is not as good as observed in earlier cases. Hence, it can be concluded that sensitivity of geometry shape variables and thickness is higher than Young's modulus and density. Hence, updating by excluding twelve shape variables did not yield in good correlation between FE and experimental results.

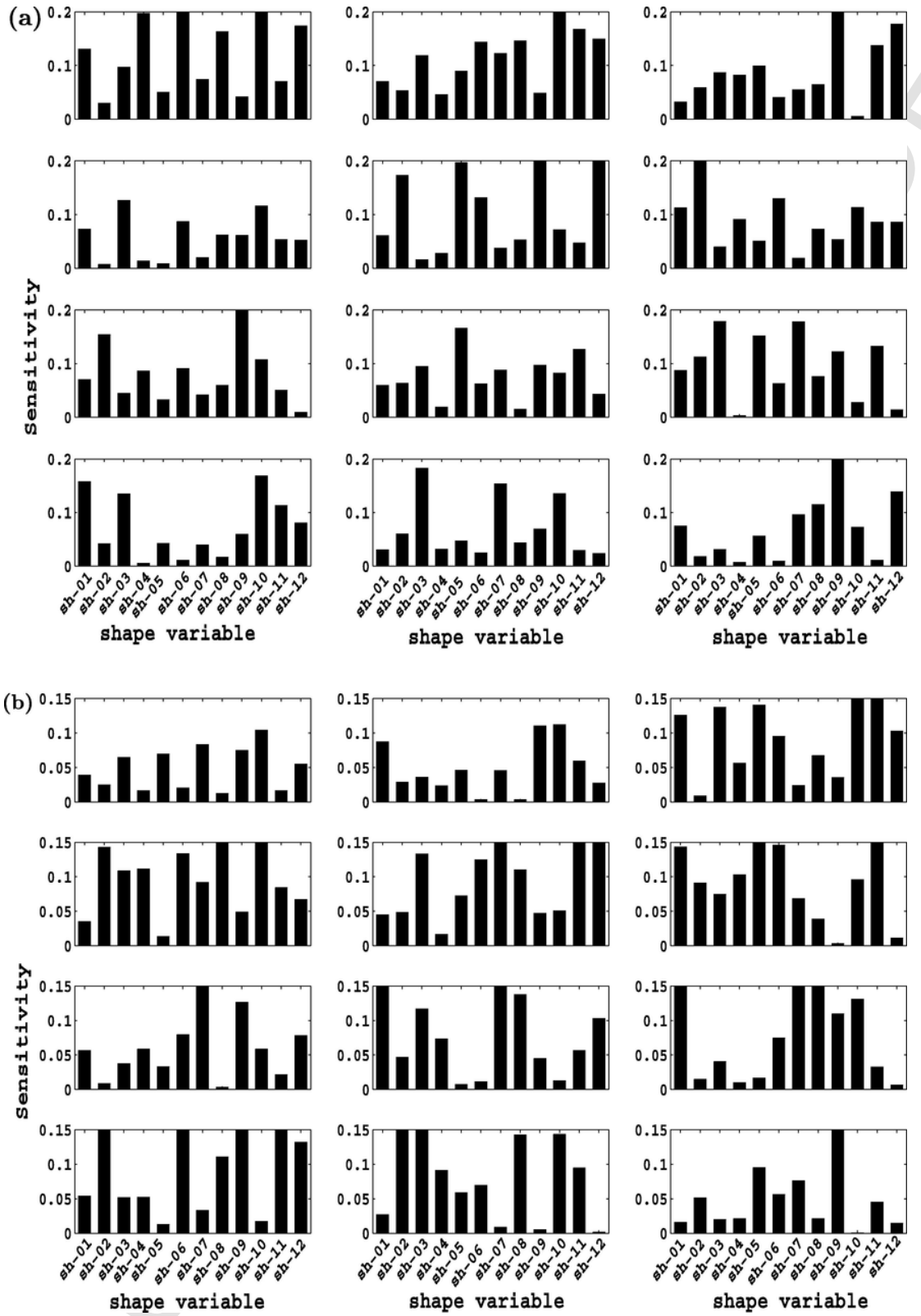

Fig. 12. Sensitivity (absolute) results of the first twelve diagonal terms of MAC matrix with respect to different geometry shape variables in (a) free-free, (b) clamped boundary conditions.

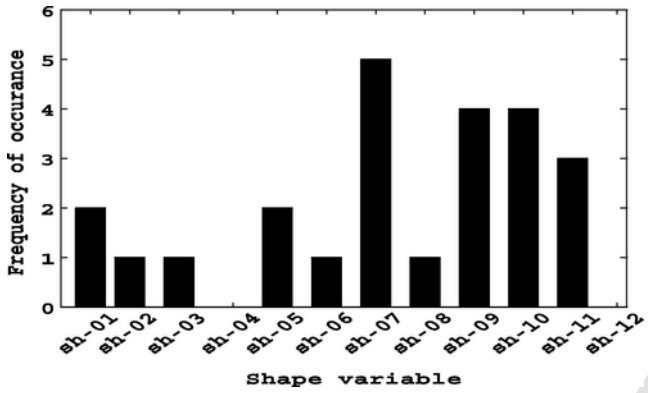

Fig. 13. Histogram of geometry shape variables of first twelve diagonal terms of MAC matrix.

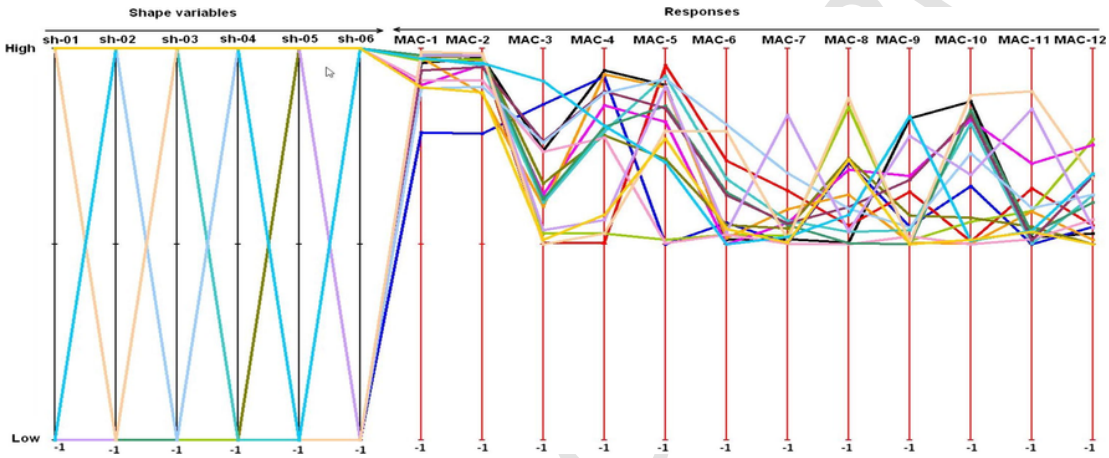

Fig. 14. Simulation results of Design of Experiments of different geometry shape variables.

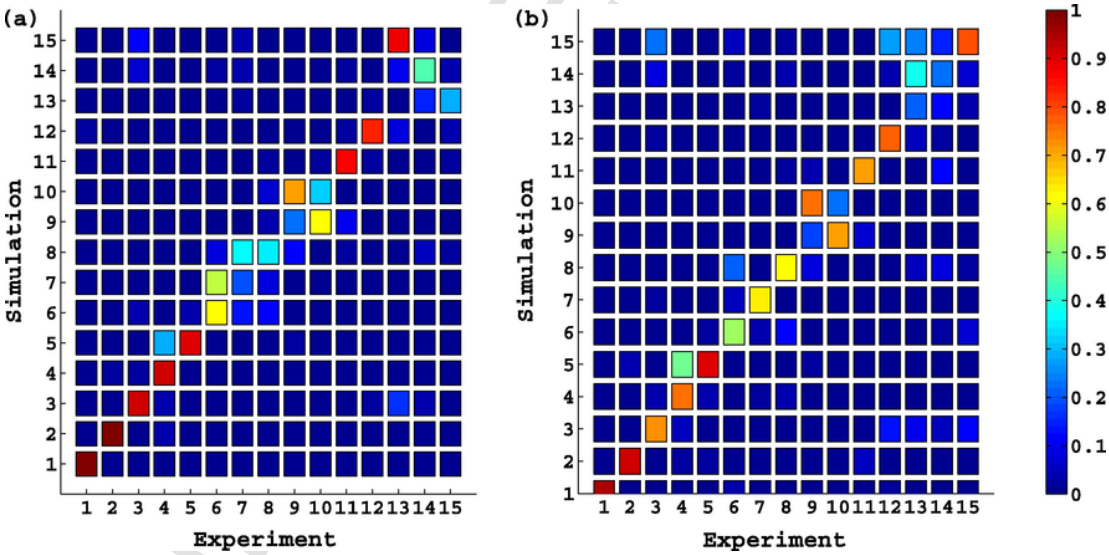

Fig. 15. Initial MAC optimization study results of (a) baseline, (b) optimized configuration in free-free boundary condition.

In order to further understand the significance of geometry shape variable effects on the optimization results, fewer design variables (identified from the sensitivity results of Fig. 13) are considered for a third optimization study. In this study, total eighteen variables – thicknesses of twelve segments and six geometry shape variables – are considered as against forty-eight variables of the

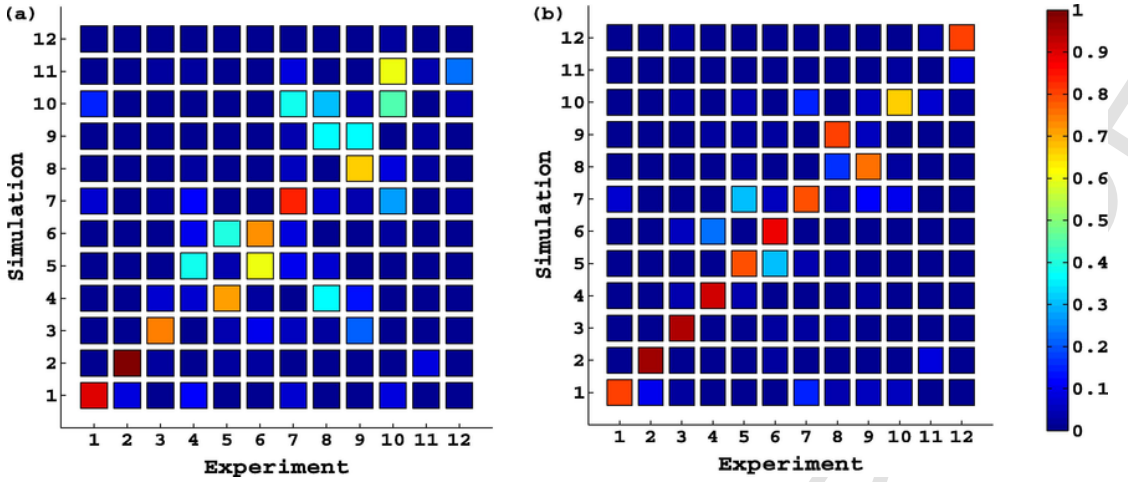

Fig. 16. Initial MAC optimization study results of (a) baseline, (b) optimized configuration in clamped boundary condition.

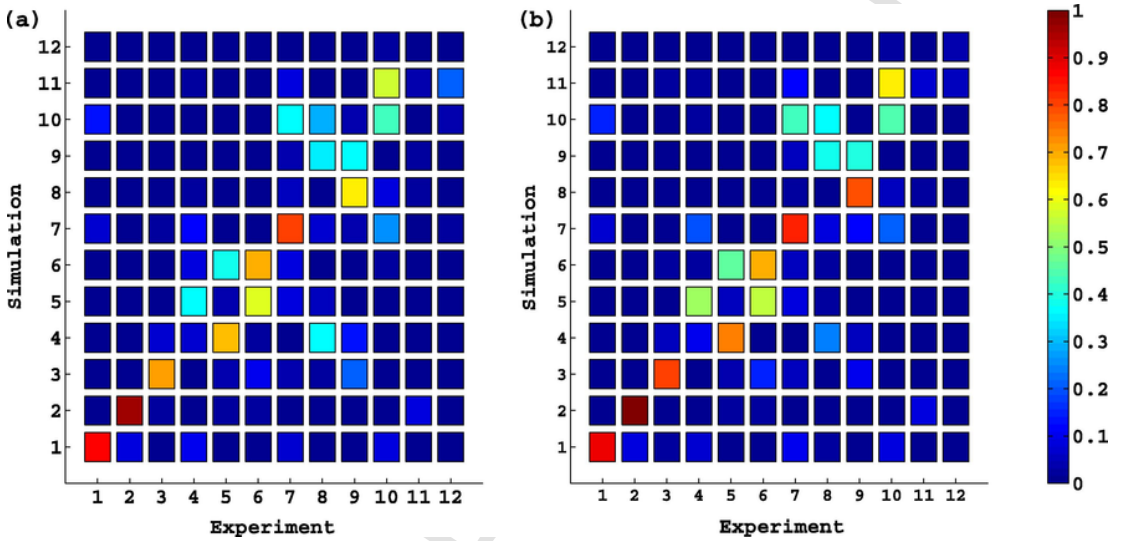

Fig. 17. MAC results of (a) baseline, (b) optimized configurations by excluding geometry variables.

initial optimization study. These results are shown in Figs. 18 and 19 for free-free and clamped boundary conditions. As can be seen from the results, 18 variables are already sufficient to arrive at good correlation (MAC values higher than 0.8) between experimental and FE results. The frequency comparison using sum of FRF as a metric is verified with optimized configuration. The comparison of sum FRFs of baseline, optimized and experimental results are shown in Fig. 20. The results show that there is a better alignment of frequencies towards experimental results, although in absolute sense there is still room for improvement. The discrepancy between numerical and experimental results may be attributed to work hardening effects that occur during manufacturing process.

In the third optimization study, where only 18 variables (12 thicknesses and 6 geometry shape variables) are considered, MAC values for some frequencies are better when compared to results of 48 variable optimization study. This can be explained by the fact that in 48 variable optimization study, geometry variables are used relatively to a lesser extent than in case of 12 variable optimization study. Table 2 confirms this fact, as the values of geometry shape variables of 18 variables study are relatively higher. Hence this confirms the need for model updating using geometric shape variables in case of deep-drawn components in order to obtain a good correlation with experimental results.

3.6. Geometry results

In this section, a novel method of obtaining a CAD surface is demonstrated. The typical process for obtaining a CAD surface through an optimization study is shown in Fig. 8. A little consideration will show that the information regarding physical form is lost after obtaining stiffness and mass matrices from a discretized finite element model. It may be noted that there can be numerous physical geometries that can give rise to very similar combination of stiffness and mass matrices. After obtaining mass and stiffness matrices, an optimization study is carried out as described in previous sections. A combination of mass and stiffness matrices

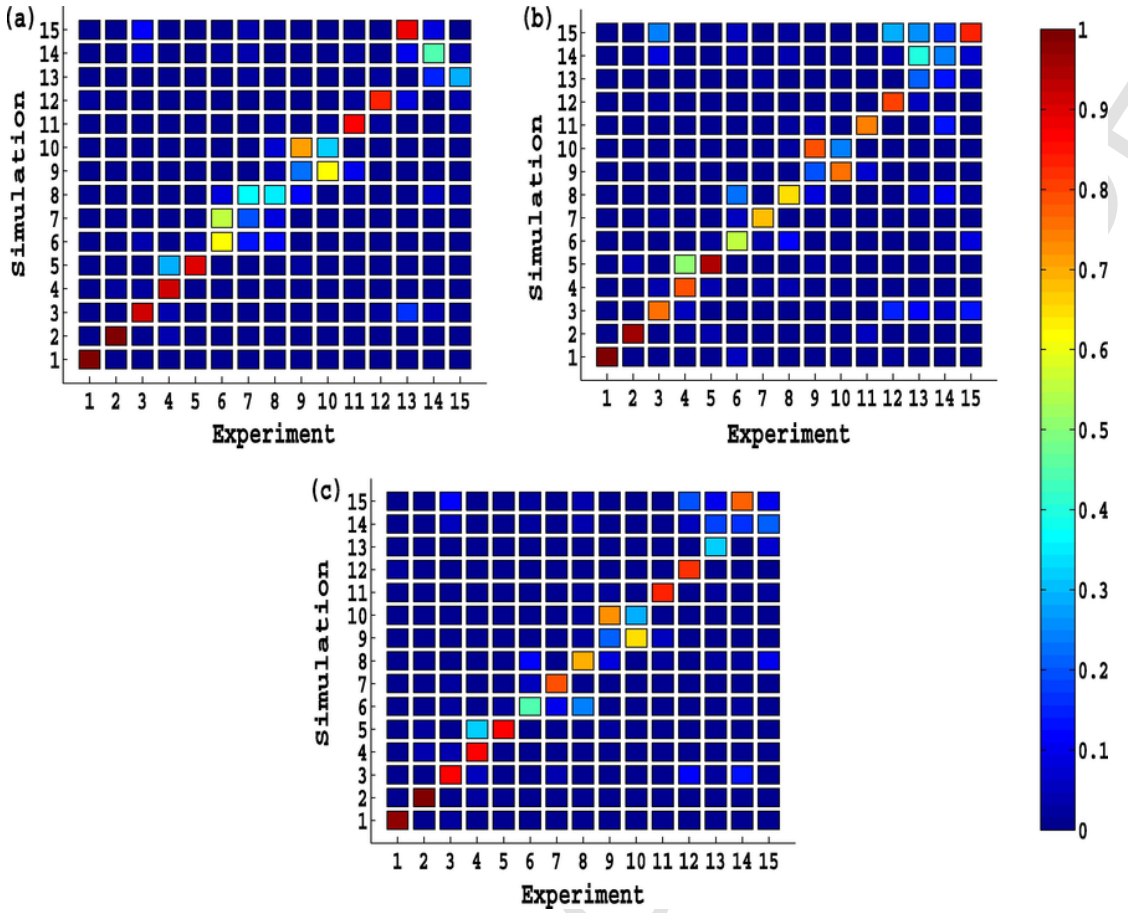

Fig. 18. Comparison of optimization results between different configurations (a) baseline, (b) 48 variables, (c) 18 variables in free-free boundary condition.

– whose frequency and mode shape correlate very well with experimental results – are arrived through an optimization study. It is possible to construct the surface from the optimized finite element model using OptiStruct. This process involves several cumbersome steps. A very brief overview of the procedure is mentioned here, as complete description falls outside the scope of this work. As an initial step, exterior faces from the finite element mesh are generated. The angle between normals of faces is used as a basis for forming edges and several such combination of edges are formed as edge-loops. A surface is fitted using the edge-loops and faces generated by finite element mesh. This geometry may be considered as a close representation of the actual part with some limitations arising out of non-uniqueness problem. As the nodal perturbations considered in the study are very small, linear behaviour is expected. Hence it may be expected that the CAD surface that is generated from the optimized finite element model, can potentially represent the actual part. In order to confirm this, a comparison of geometrical deviation between the CAD model generated from the optimized finite element model and scanned CAD model is done at ten different sections, spanning entire length of component. These results are shown in Fig. 21. As can be seen from the figure, that the maximum deviation of the optimized scanned model from the actual part is 2.7 mm. This is considerably lower than the deviation between original CAD and scanned CAD models which is 5.3 mm. Hence it can be concluded that CAD surface obtained through this process, by-and-large, can represent the actual part which obviates the need of scanning the actual part in order to obtain the actual part CAD surface.

In this context of geometry updating it is worth mentioning IsoGeometric Analysis (IGA) [31,32] as a promising analysis tool that could allow to significantly speed up the model updating process. IGA is a generalization of the FEM which uses the spline-based descriptions embedded in the CAD geometry as shape functions for the analysis process. In doing so, both the geometry and the deformation variables are represented by the same spline-based descriptions. This intrinsic integration of geometry and analysis offers several advantages. Firstly, it makes the translation step from optimized FE model to corresponding CAD model redundant, as the optimized IGA model is expressed directly in terms of the CAD shape parameters. Secondly, this parametric shape description is much more efficient (and intuitive) in describing the product geometry than the nodal definition of a FE mesh, which could be exploited when defining the shape variables. And thirdly, it obviates the need of creating a mesh of the CAD model in order to obtain an analysis-suitable geometry, thereby significantly reducing pre-processing times for complex-shaped products. Moreover, the smoother character of spline-based functions has been shown to yield important advantages with regard to computational efficiency, in particular for solving dynamic problems [33–35]. In fact, IGA has already been studied extensively and applied successfully to a

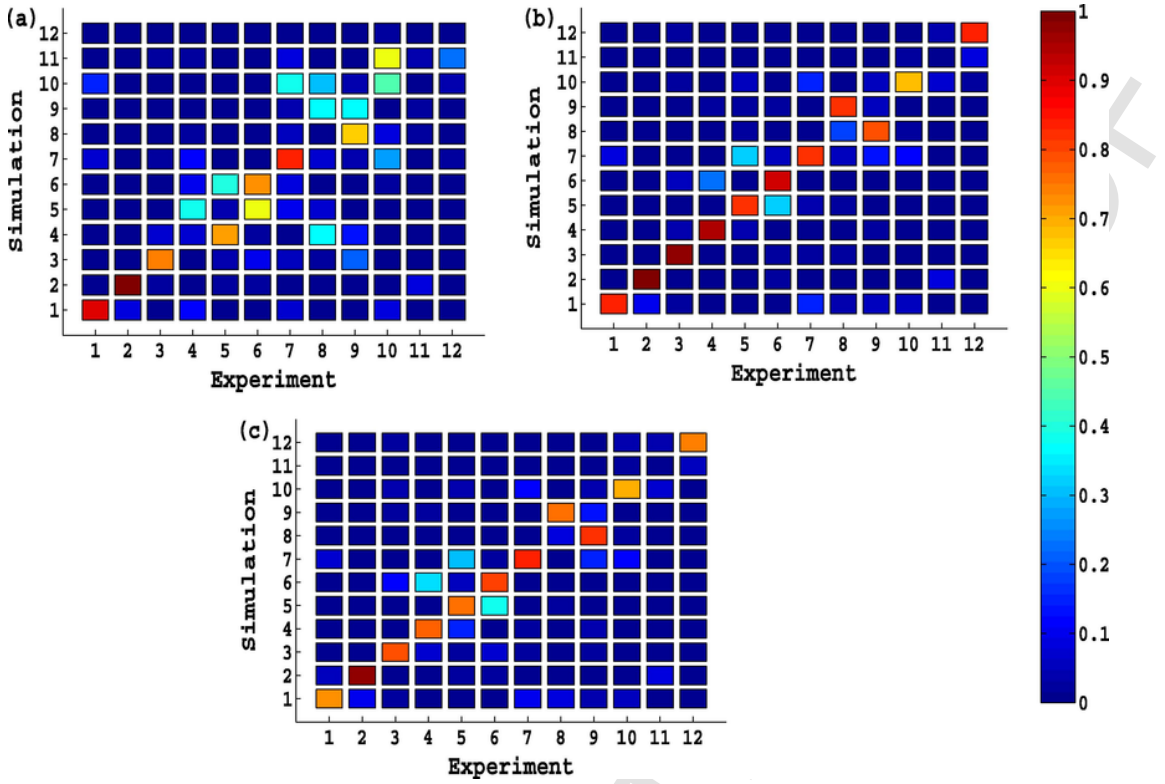

Fig. 19. Comparison of optimization results between different configurations (a) baseline, (b) 48 variables, (c) 18 variables in clamped boundary condition.

multitude of problem types, amongst others in shape optimization procedures [36,37]. The authors believe that the integration of IGA into the proposed model updating procedure is a promising future research work.

4. Conclusions

A comprehensive methodology is developed to update finite element models of deep-drawn components. It is shown that in case of components that are manufactured with high draw ratios – where significant profile deviation and thickness variations take place – only material property updating will not yield the desired accuracy for correlating with experimental results. Hence it is proposed that shape variables which depict the likely geometrical changes that can happen during manufacturing of components are used for optimization study. It is shown by taking these geometrical shape variables into consideration, an improved correlation between finite element and experimental results is achieved. It is also shown that as nodal perturbations are small, it is possible to arrive at the geometry that deviates a lot lesser from the actual part than the original CAD geometry does. This method obviates the need of scanning the actual part to obtain the geometry and then to arrive at a dynamic-equivalent finite element model.

Acknowledgements

The authors gratefully acknowledge the help received from the colleagues at PMA section of KU Leuven and the members at Noise, Vibration and Harshness laboratory of TVS Motor Company. The research work of Elke Deckers is financed by a post-doctoral grant of the Research Foundation Flanders (FWO). The authors would also like to sincerely thank Mr. N. Jayaram, Vice President of Research and Development and Mr. Vinay Harne, President, New Product Introduction (NPI) of TVS Motor Company for providing support and facilities to carry out this work.

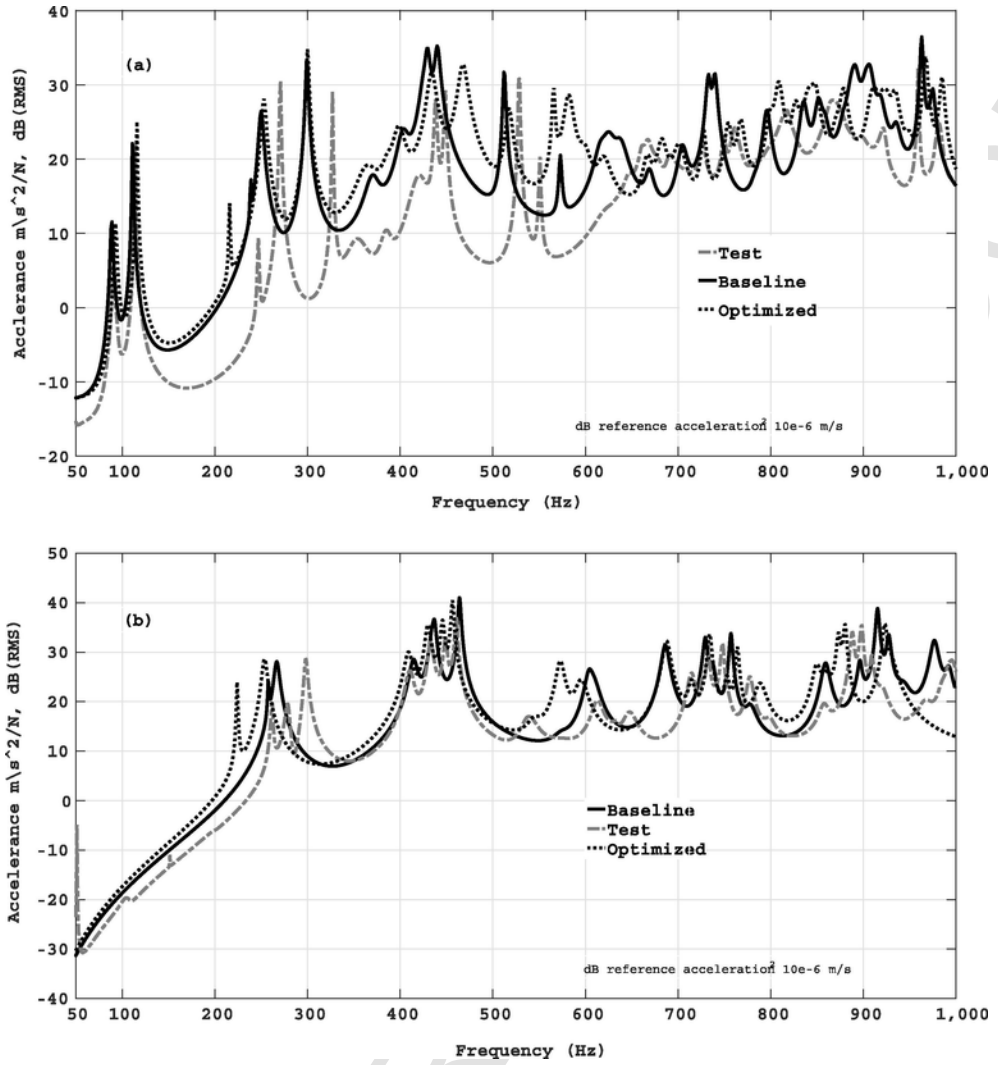

Fig. 20. Comparison of sum Frequency Response Functions(FRF) between baseline, optimized simulations and experimental results in (a) free-free, (b) clamped boundary conditions.

Table 2
Comparison of absolute normal displacement (mm) of geometry shape variable values between 48 variables and 18 variables optimization studies.

Shape variable	48 variables study	18 variables study
sh-01	1.14	1.37
sh-02	1.36	1.55
sh-03	0.31	1.12
sh-04	0.96	1.38
sh-05	0.51	1.15
sh-06	1.45	2.51
sh-07	0.12	–
sh-08	0.02	–
sh-09	0.08	–
sh-10	0.14	–
sh-11	0.09	–
sh-12	0.00	–

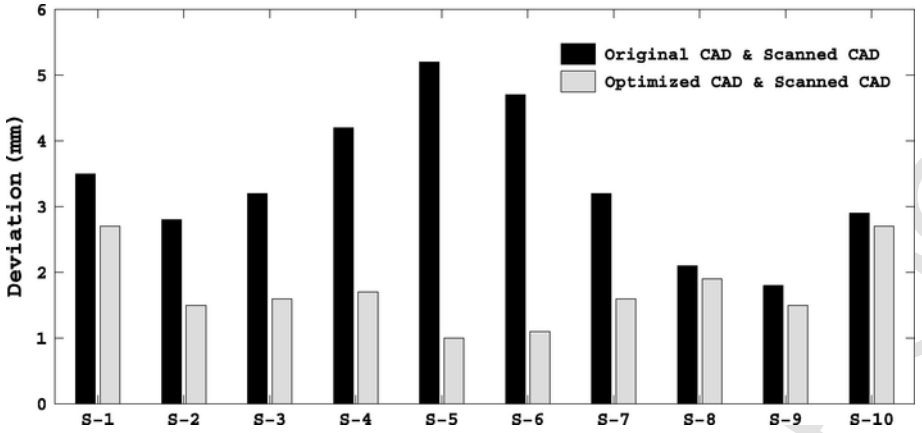

Fig. 21. Comparison of geometry profile deviation of the optimized CAD model with respect to scanned CAD model.

References

[1] O. Zienkiewicz, R. Taylor, D. Fox, The Finite Element Method for Solid and Structural Mechanics, Elsevier, Oxford, 2013.
[2] J. Mottershead, M. Friswell, Model updating in structural dynamics: A survey, J. Sound Vib. 167 (2) (1993) 347–375.
[3] J. Mottershead, M. Friswell, G. Ng, et al., Geometric parameters for finite element model updating of joints and constraints, Mech. Syst. Signal Process. 10 (2) (1996) 171–182.
[4] Z. Yuan, K. Yu, Finite element model updating of damped structures using vibration test data under base excitation, J. Sound Vib. 340 (2015) 303–316.
[5] N. Guo, Z. Yang, Y. Jia, L. Wang, Model updating using correlation analysis of strain frequency response function, Mech. Syst. Signal Process. 70–71 (2016) 284–289.
[6] C. Maletta, L. Pagnotta, On the determination of mechanical properties of composite laminates using genetic algorithms, Int. J. Mech. Mater. Des. 1 (2004) 199–211.
[7] V. Meruane, Model updating using antiresonant frequencies identified from transmissibility functions, J. Sound Vib. 332 (2013) 807–820.
[8] G. Petrone, V. Meruane, Mechanical properties updating of a non-uniform natural fibre composite panel by means of a parallel genetic algorithm, Compos. A 94 (2017) 226–233.
[9] A. Andersson, Numerical and experimental evaluation of springback in a front side member, J. Mater. Process. Technol. 169 (2005) 352–356.
[10] W. Hancock, M. Zayko, M. Autio, D. Ponagajba, Analysis of components of variation in automotive stamping processes, Quality Eng. 10 (1) (1997) 115–124.
[11] H. Kim, H. Jung, J. Cho, W. Bae, Finite element analysis on process improvement of the multi-forming for the motor-case of an automobile, J. Mater. Process. Technol. 187–188 (2007) 378–382.
[12] T. de Souza, B.F. Rolfe, Characterising material and process variation effects on springback robustness for a semi–cylindrical sheet metal forming process, Int. J. Mech. Sci. 52 (2010) 1756–1766.
[13] R. Padmanabhanan, M. Oliveira, J. Alves, L. Menezes, Numerical simulation and analysis on the deep drawing of LPG bottles, J. Mater. Process. Technol. 200 (2008) 416–423.
[14] M.E. Mouatassim, J. Jameux, B. Thomas, F. Mehrez, G. Milcent, The simulation of multi-operation deep-drawing process at renault with pam stamp, J. Mater. Process. Technol. 45 (1994) 317–322.
[15] The MathWorks, Inc, MATLAB 2012b, *User Guide*, 2012.
[16] D. Ewins, Modal Testing, Research Studies Press, 1984.
[17] W. Heylen, P. Avitabile, Correlation considerations – Part 5 (degree of freedom correlation techniques), In: 16th International Modal Analysis Conference, Santa Barbara, USA, 1998.
[18] J. O'Callahan, Correlation considerations – Part 4 (modal vector correlation techniques), In: 16th International Modal Analysis Conference, Santa Barbara, USA, 1998.
[19] R. Allemang, D. Brown, A correlation coefficient for modal vector analysis, In: 1st International Modal Analysis Conference, Orlando, USA, 1982.
[20] M. Baruch, Optimisation procedure to correct stiffness and flexibility matrices using vibrtaion tests, AIAA J. 16 (11) (1978) 1208–1210.
[21] A. Berman, E.J. Nagy, Improvement of a large analytical model using test data, AIAA J. 21 (8) (1983) 1168–1173.
[22] R.L. Fox, M.P. Kapoor, Rate of change of eigenvectors and eigenvalues, AIAA J. 12 (6) (1968) 2426–2429.
[23] H. Grafe, Model updating of large structural dynamics models using measured response functions, Ph.D. thesis Department of Mechanical Engineering, 1998.
[24] J.C. Chen, J.A. Garba, Analytical model improvement using modal tests, AIAA J. 18 (6) (1980) 684–690.
[25] D. Sieger, S. Menzel, M. Botsch, Constrained space deformation for design optimization, Proc. Eng. 12 (6) (2014) 1–13.
[26] M. Meyer, M. Desbrun, P. Schrder, A.H. Barr, Discrete differential-geometry operators for triangulated 2-manifolds, in: H.-C. Hege, K. Polthier (Eds.), Visualization and Mathematics III, Springer-Verlag, Heidelberg, 2003, pp. 35–57.
[27] Altair Hyperworks software, OptiStruct 11.0 *User Guide*, 2011.
[28] GOM ATOS Professional Software Manual, 2010.
[29] Siemens PLM Software Inc, LMS SCADAS, *LMS SCADAS brouchure,* 2015.
[30] Siemens PLM Software Inc, Test.Lab 15A, *LMS Test.Lab Signature Acquisition, User Guide*, 2015.
[31] T.J.R. Hughes, J. Cottrell, Y. Bazilevs, Isogeometric analysis: CAD, finite elements, NURBS, exact geometry and mesh refinement, Comput. Methods Appl. Mech. Eng. 194 (2005) 4135–4195.
[32] V.P. Nguyen, C. Anitescu, S.P. Bordas, T. Rabczuk, Isogeometric analysis: an overview and computer implementation aspects, Mathe. Comput. Simul. 117 (2015) 89–116.
[33] T.J.R. Hughes, J.A. Evans, A. Reali, Finite element and NURBS approximations of eigenvalue, boundary-value and initial-value problems, Comput. Methods Appl. Mech. Eng. 272 (2014) 290–320.
[34] L. Coox, E. Deckers, D. Vandepitte, W. Desmet, A performance study of NURBS-based isogeometric analysis for interior two-dimensional time-harmonic acoustics, Comput. Methods Appl. Mech. Eng. 305 (2016) 441–467.
[35] L. Coox, O. Atak, D. Vandepitte, W. Desmet, An isogeometric indirect boundary element method for solving acoustic problems in open-boundary domains, Comput. Methods Appl. Mech. Eng. 316 (2016) 186–208.
[36] J. Kiendl, R. Schmidt, R. Wüchner, K.-U. Bletzinger, Isogeometric shape optimization of shells using semi-analytical sensitivity analysis and sensitivity weighting, Comput. Methods Appl. Mech. Eng. 274 (2014) 148–167.

[37] D. Nguyen, A. Evgrafov, A. Gersborg, J. Gravesen, Isogeometric shape optimization of vibrating membranes, Comput. Methods Appl. Mech. Eng. 200 (2011) 1343–1353.